15. Frank, J., King, A. R. & Raine, D. J. *Accretion Power in Astrophysics*, Ch. 5, 76 (Cambridge University Press, (1985).
16. Day, C. S. R., Fabian, A. C., George, I. M. & Kunieda, H. *Mon. Not. R. astr. Soc.* **247,** 15P (1990).
17. Acosta-Pulido, J. A., Pérez-Fournon, I., Calvani, M. & Wilson, A. S. *Astrophys. J.* **365,** 119 (1990).
18. Abramowicz, M. A., Jaroszyński, M. & Sikora, M. *Astr. Astrophys.* **63,** 221 (1978).
19. Netzer, H. in *Active Galactic Nuclei* (eds Courvoisier, T. J.-L. K., Mayer, M.) 58 (Springer, Berlin, 1990).
20. Laor, A. & Netzer, H. *Mon. Not. R. astr. Soc.* **238,** 897 (1990).
21. Padovani, P. *Astr. Astrophys.* **209,** 27 (1989).
22. Sun, W.-H. & Malkan, M. A. *Astrophys. J.* **346,** 68 (1989).
23. Wandel, A. in *Proc. IAU Symp. No.* 134, *Active Galactic Nuclei* (Kluwer, Dordrecht, 1989).
24. Bath, G. T., Evans, W. D. & Papaloizou, J. *Mon. Not. R. astr. Soc.* **167,** 7P (1974).
25. Mittaz, J. P. D. & Branduardi-Raymont, G. *Mon. Not. R. astr. Soc.* **238,** 1029 (1989).
26. Zelik, M., Hall, D. S., Deldman, P. A. & Walter, F. *Sky Telesc.* **57,** 132 (1979).
27. McWilliams, J. C. *J. Fluid Mech.* **219,** 361 (1990).
28. Meacham, S. P., Flierl, G. R. & Send, U. *Dyn. Atmos. Oceans* **14,** 333–386 (1990).
29. McWilliams, J. C. *J. Fluid Mech.* **146,** 21 (1984).
30. Maltrud, M. E. & Vallis, G. K. *J. Fluid Mech.* **228,** 321 (1991).
31. Rhines, P. B. & Young, W. R. *J. Fluid Mech.* **122,** 347 (1984).
32. Ingersoll, A. P. & Cuong, P. G. *J. atmos. Sci.* **38,** 2067 (1981).
33. Williams, G. P. & Wilson, R. J. *J. atmos. Sci.* **45,** 207 (1988).
34. Marcus, P. S. *J. Fluid. Mech.* **215,** 393–430 (1990).
35. Sommeria, J., Nore, C., Dumont, T. & Robert, R. *C.R. Acad. Sci. Paris* **312,** 999–1005 (1991).
36. Qian, Z., Spiegel, E. A. & Proctor, M. R. E. *Stab. Appl. Anal. Cont. media* **1,** 73 (1991).
37. Ting, A. C., Matthaeus, W. H. & Montgomery, D. *Phys. Fluids* **29,** 3261 (1986).
38. Silaev, I. I. & Skvortsov, A. T. in *Nonlinear World* 2 (eds Bar'yakhtar, V. G., Chernousenko, V. S., Erokhin, N. S., Sitenko, A. G. & Zakharov, V. E.) 1007 (World Scientific, Singapore, 1990).

ACKNOWLEDGEMENTS. We thank S. Meacham and W. Young for discussions, and N. Balmforth for reading the manuscript. M.A.A., A.L. and E.S. acknowledge the financial support of NORDITA, and E.A.S. acknowledges NSF for financial support.

The thermal stability of near-surface ground ice on Mars

David A. Paige

Department of Earth and Space Sciences, University of California, Los Angeles, Los Angeles, California 90024, USA

THE existence of subsurface water ice on Mars has been predicted in several theoretical studies[1–5], but there are no definitive observations of its present distribution. Geomorphic features on the surface of Mars have been widely interpreted as evidence for the presence of ground ice[6–12], but many of these features are found at near-equatorial latitudes, where thermal models have predicted that near-surface water ice should not be stable under present climate conditions[3,13,14]. Here I present the results of thermal calculations which show that observed geographic variations in the thermal and reflectance properties of martian soils significantly affect subsurface temperatures. My results indicate that in certain regions, ground-ice deposits could exist much closer to the surface, and much closer to the equator, than previously thought. In the future, these deposits could be a valuable resource for human exploration[15].

The thermal and reflectance properties of mid-latitude surface materials are highly non-uniform. Viking infrared thermal mapper (IRTM) observations[16] show that the apparent thermal inertia of the martian surface ranges from 46 to 630 J m^{-2} s$^{-1/2}$ K^{-1}. Thermal inertia is a composite quantity defined as $I = \sqrt{k\rho c}$, where k is the thermal conductivity, ρ is the density and c is the heat capacity. As the product ρc for all geological materials varies by less than a factor of three, the thermal conductivity of martian soil must vary by more than two orders of magnitude. Of particular interest are the three large regions of low thermal inertia centred at (+20° N, 120° W), (+15° N, 330° W) and (+20° N, 215° W), which correspond geographically to the classical bright regions of Tharsis, Arabia and Elysium. Analysis of the available remote sensing data indicates that the surfaces of these regions differ markedly from those observed at close range at the Viking landing sites[17], in that they are uniformly blanketed by a layer of thermally insulating, fine-grained dust, 0.1–0.2 m thick[18].

Figure 1 shows the results of thermal model calculations of annual minimum, maximum and average surface temperatures as a function of latitude for 'Mars average', 'high-thermal-inertia' and 'low-thermal-inertia' soils. Annual maximum surface temperatures are higher in the southern hemisphere because the eccentricity of the orbit of Mars brings it closer to the Sun during the southern spring and summer seasons. Soils with low thermal inertia experience higher annual maximum and lower annual minimum temperatures because the amplitudes of their daily surface temperature variations are larger. Predicted annual minimum surface temperatures are 148 K for low-thermal-inertia soils in the equatorial regions because transient, pre-dawn surface CO_2 frost forms during the coldest seasons. At higher latitudes, annual minimum surface temperatures of 148 K are due to the formation of the north and south seasonal CO_2 polar caps. Annual average surface temperatures are lower for soils with lower thermal inertia because they emit a greater proportion of their energy at infrared wavelengths near midday, when surface temperatures are near maximum. This nonlinear diurnal effect vanishes near the poles where diurnal temperature variations are absent. If the effects of subsurface heat flow are neglected, then calculated annual average surface temperatures will be the expected annual mean temperatures at depth.

Thermal model calculations of subsurface temperatures can be used to determine the expected depths of ground-ice deposits because near-surface water ice will not be stable to evaporation if temperatures exceed the local frost-point temperature for extended periods. Farmer and Doms[13] have used observations of total column water abundances made by the Viking Mars

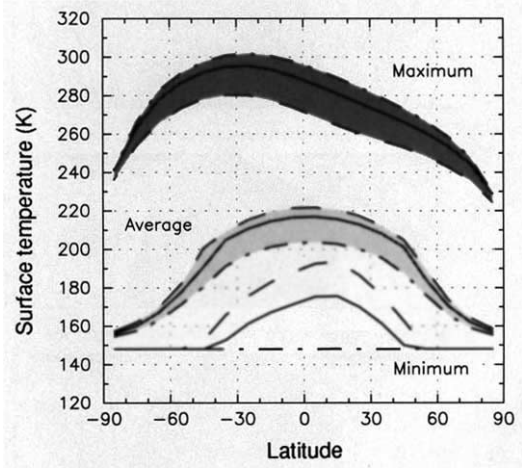

FIG. 1 Calculated annual minimum, maximum and average surface temperatures for 'Mars average' (solid line), 'high thermal inertia' (dashed) and 'low thermal inertia' (dot-dashed) soil thermal and reflectance properties. The thermal model used here is similar in concept to the original model of ref. 3, and to models that have been used subsequently[30,31]. During each model timestep, the one-dimensional heat-diffusion equation is solved to calculate surface and subsurface temperatures, and if appropriate, surface CO_2 frost condensation or sublimation rates. Carbon dioxide frost temperatures were fixed at 148 K, CO_2 frost albedos were fixed at 0.65, and all surfaces were assumed to have unit emissivities at infrared wavelengths. A small upward heat-flow rate from the martian interior of 0.03 W m^{-2} was also assumed[32]. The effects of atmospheric radiation on the surface energy balance were not calculated explicitly, but were accounted for by assuming that the surface is heated by the atmosphere throughout the day at a rate of 2% of the local noontime insolation, or 2% of the frost thermal emission during the polar night, whichever is greater[19]. The same assumption has been used to derive best-fit apparent thermal inertias and albedos from IRTM brightness temperature observations[16,19]. The thermal inertias I and albedos A for 'Mars average', 'high-thermal-inertia' and 'low-thermal-inertia' soils are taken to be (I = 272 J m^{-2} s$^{-1/2}$ K^{-1}, A = 0.25), (I = 630 J m^{-2} s$^{-1/2}$ K^{-1}, A = 0.25) and (I = 85 J m^{-2} s$^{-1/2}$ K^{-1}, A = 0.30) respectively[16,30]. The product ρc was assumed to be 1.00464 J m^{-2} K^{-1} for all cases. Soil thermal and reflectance properties were verified by using the same thermal model employed in this study to fit the available IRTM 20-μm channel brightness temperature data obtained between −20° N and +40° N over the complete diurnal cycle at a spatial resolution of ~100 km. For best-fit apparent thermal inertias between 80 and 90 J m^{-2} s$^{-1/2}$ K^{-1}, the average best-fit albedo was 0.301 with a standard deviation of 0.038.

atmospheric water detector to estimate that in the equatorial and temperature latitudes, near-surface frost-point temperatures are ~198 K. This estimate assumes that the observed water vapour is mixed uniformly with pressure throughout the atmospheric column. The temperatures of near-surface ground-ice deposits could exceed 198 K and still be consistent with observed column water-vapour abundances if water-vapour mixing ratios are higher near the surface than they are for the atmospheric column as a whole. For instance, a surface frost-point temperature of 203 K could be supported by 15 precipitable micrometres of total atmospheric water vapour distributed uniformly with pressure from the surface to an altitude of 8 km.

Figure 2*a–c* shows contours of annual maximum and minimum subsurface soil temperatures calculated for the same three sets of model input parameters used to calculate surface temperatures in Fig. 1. The results using the 'Mars average' thermal and reflectance properties in Fig. 2*a* are qualitatively similar to those of previous studies[3,13,14], which predict that ground ice should be stable from the poles to latitudes of roughly ±45°. The results in Fig. 2*b* show that for regions with high thermal inertia, the region of permanent ice stability should lie further below the surface and closer to the poles. The boundary is deeper because depths of penetration of diurnal and seasonal temperature waves increase as the square root of the thermal diffusivity[19,20]. The region of permanent ice stability is further from the equator for high-inertia soil because of the nonlinear effects of thermal inertia on average temperatures discussed above. The results in Fig. 2*c* show that for regions of low thermal inertia and high albedo, the permafrost boundary is expected to lie closer to the surface, and closer to the equator.

An important question not considered previously is whether the formation of martian ground ice is thermally stable. To investigate, I did another set of calculations in which the thermal inertias of subsurface soil layers below the first diurnal skin depth were slowly increased as long as their temperatures remained below the frost point to simulate the formation of interstitial ice. If the temperatures of these layers ever exceeded the frost point, their thermal inertias were rapidly decreased to simulate ice sublimation. Figure 2*d* and *e* shows the results after 120 years for a global frost-point temperature of 198 K. Figure 2*d* assumes thermal and reflectance properties for 'Mars average' ice-free soil, like those used in Fig. 1*a*. Figure 2*e* assumes properties for 'low-thermal-inertia' ice-free soil, like those used in Fig. 2*c*. The results reveal that once formed, high-thermal-inertia ice deposits can be stable much closer to the surface than has been predicted by earlier models.

The stability of ground ice deposits near the surface can be explained by the tendency of the overlying ice-free surface layer

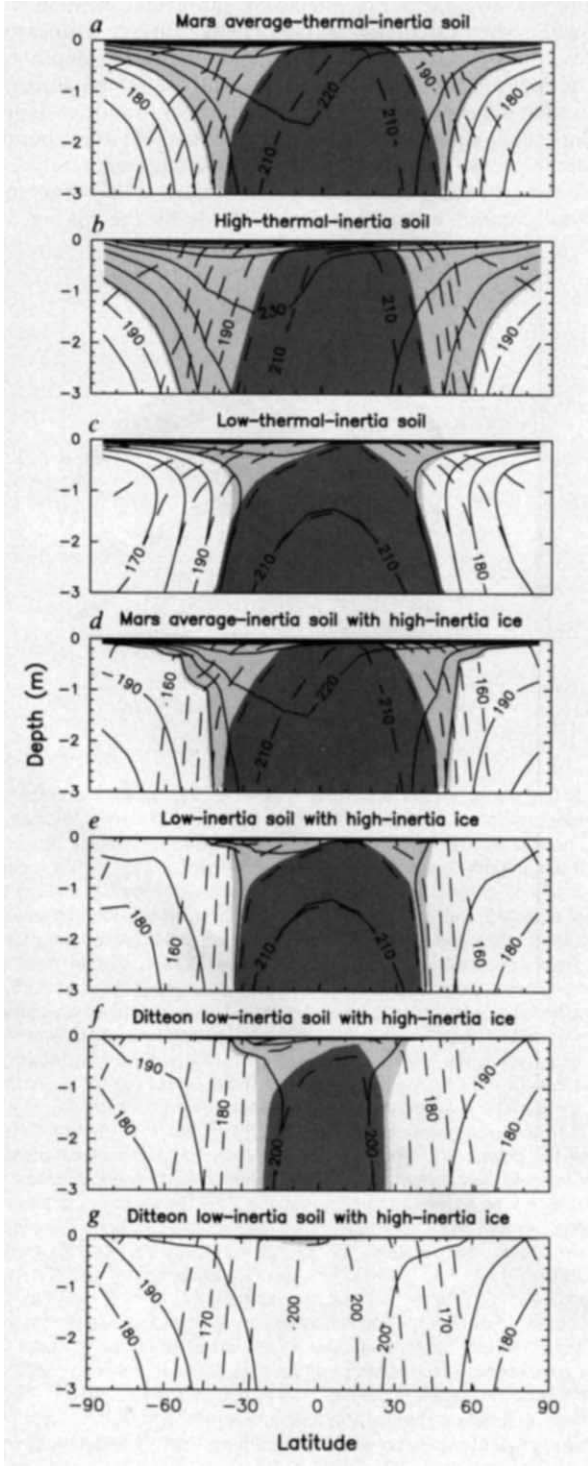

◀ FIG. 2 Contours of model-calculated annual minimum (dashed line) and annual maximum (solid) temperatures as a function of latitude and depth. White, unshaded areas denote regions of permanent ground-ice stability, where temperatures never exceed the frost-point temperature. Lightly shaded areas denote regions of temporary ground-ice stability, where temperatures exceed the frost point during part of the year. Dark shaded areas denote the permanently frost-free regions, where temperatures always exceed the frost point. *a–c*, Ground-ice stability boundaries for vertically homogeneous 'Mars average', 'high-thermal-inertia', and 'low-thermal-inertia' soils assuming a frost-point temperature of 198 K. *d*, *e*, Ground-ice stability boundaries for 'Mars average' and 'low-thermal-inertia' soils overlying subsurface soil layers whose thermal properties were allowed to vary with time. At the start of the calculations, subsurface soil layers were assumed to be ice-free, and subsurface thermal properties were assumed to be uniform with depth. Each day, the thermal inertias of subsurface layers below the first diurnal skin depth were modified to simulate the formation or sublimation of interstitial ice. If a layer's daily maximum temperature was lower than the frost-point temperature of 198 K, its thermal inertia was slowly increased. The timescale for complete ice saturation was assumed to be 20 Mars years, which is long enough to cause negligible variations in soil thermal properties over diurnal and seasonal timescales. Layer thermal inertias were allowed to increase until they reached a maximum value of 1,256 J m^{-2} s$^{-1/2}$ K^{-1}, which is ~3/5 the expected thermal inertia of pure solid water ice. If a layer's daily maximum temperature was higher than the frost-point temperature, then its thermal inertia was rapidly decreased to simulate ice sublimation. The timescale for complete sublimation was assumed to be 20 days. Experimentation showed that the results of these simulations were relatively insensitive to the timescales assumed, as long as the rates of ice condensation were assumed to be much longer than the rates of ice sublimation, which is likely to be the case because of the exponential dependence of equilibrium vapour pressure on temperature. *f*, *g*, Same as *d* and *e*, but using Ditteon's two-layer thermal and reflectance properties for low-thermal-inertia soil (I = 79 J m^{-2} s$^{-1/2}$ K^{-1}, A = 0.344), which provide a better fit to the IRTM brightness temperature observations[21]. *f* assumes a frost-point temperature of 198 K, whereas *g* assumes a frost-point temperature of 203 K.

to decrease average temperatures at depth while simultaneously insulating deeper layers from large-amplitude temperature variations. As long as the ice-free surface layer extends to a diurnal skin depth below the surface, the presence of high-thermal-inertia material below the surface has only second-order effects on diurnal variations in surface temperature. This means that, to first order, the properties of the ice-free surface soil layer control the daily average surface temperature and, at mid-latitudes, the annual average temperatures at depth. At latitudes where annual maximum subsurface temperatures are lower than the frost point, ice formation increases the thermal inertia and thermal diffusivity of subsurface soil layers. This causes the heat that is being conducted into these layers from above to be distributed deeply over a large thermal mass, decreasing the temperature variations that these layers experience, and promoting further ice formation. As the thermal inertias of the icy layers increase, they can migrate upward towards the surface by reducing the amplitudes of temperature variations in adjacent ice-free layers. As all of these effects tend to accelerate with increasing thermal inertia, martian ground-ice deposits would be expected to maximize their thermal inertias if water is available, and become fairly solid.

Actual ground-ice boundaries on Mars could deviate considerably from those calculated here because of variations and uncertainties in both the frost-point temperature and the thermal behaviour of the soil itself. The sensitivity of these boundaries can be demonstrated as follows. In low-thermal-inertia regions, measured infrared brightness temperatures at 6 p.m. local time can be more than 20 K colder than the temperatures predicted by simple homogeneous thermal models. Ditteon[21] has fitted daily temperature variations observed over a complete diurnal cycle for a region in Tharsis to a r.m.s. accuracy of 3.14 K, using a thermal model that assumes a thin surface layer of bright low-thermal-inertia material overlying a deep layer of high-thermal-inertia material, which Ditteon attributed to the presence of duracrust or rock. When the same thermal model used in Fig. 2*d* and *e* is initialized using Ditteon's best-fit surface soil properties, but assuming that the high-thermal-inertia material below the surface is ground ice, the results in Fig. 2*f* are obtained. Increasing the assumed frost point from 198 K to 203 K gives the results shown in Fig. 2*g*, which would predict that near-surface ground ice is stable at the equator. Although Ditteon's parameters provide an improved fit to the IRTM observations, his explanation for the anomalously cold afternoon brightness temperatures is not unique, as they can be explained satisfactorily in many regions by the effects of diurnal variations in the rates of radiative and convective heat transfer between surface and atmosphere[22]. The extreme sensitivity of the results presented here suggests that a more complete treatment of all factors that influence subsurface temperatures and abundances of near-surface water vapour should be included in considerations of the stability of ground ice close to the equator.

Determining the present distribution of near-surface ground ice on Mars will be a prime objective for future spacecraft missions. Definitive evidence for its presence at low latitudes would enhance the prospects for human exploration and habitation. These results show that, all things being equal, low-thermal-inertia regions will be the most favourable locations for near-surface water-ice deposits. At present, low-latitude ground ice could be widespread within the Tharsis, Arabia and Elysium low-thermal-inertia regions. Over long timescales, the stability of ice in low-thermal-inertia regions is likely to be intimately linked with the martian climate, as the behaviour of both dust and water on Mars should be strongly affected by quasiperiodic variations in Mars's orbital and axial elements[23]. In this respect, these regions may be similar to the layered deposits of dust and ice observed near the north and south poles[24]. Although the nature of the martian environment during other climate epochs is difficult to predict, the possible stability of near-surface ground ice in low-thermal-inertia regions on Mars today might help resolve a number of long-standing problems relating to the presence of low-latitude ice-related geomorphic features[6-12,23,25-27], and the possible involvement of ground ice in low-latitude sedimentary[28] and fluvial processes[29]. □

Received 23 September 1991; accepted 23 January 1992.

1. Lebedinsky, A. I. *Rep. Acad. Sci. USSR* **108,** 795-798 (1956).
2. Lederberg, J. & Sagan, C. *Proc. Natn. Acad. Sci. USA* **48,** 1473-1475 (1962).
3. Leighton, R. B. & Murray, B. C. *Science* **153,** 136-144 (1966).
4. Anderson, D. M., Gaffney, E. S. & Law, P. F. *Science* **155,** 319-322 (1967).
5. Smoluchowski, R. *Science* **159,** 1348-1350 (1968).
6. Sharp, R. P., Soderblom, L. A., Murray, B. C. & Cutts, J. A. *J. geophys. Res.* **76,** 331-342 (1971).
7. Sharp, R. P. *J. geophys. Res.* **78,** 4073-4083 (1973).
8. Carr, M. H. & Schaber, G. G. *J. geophys. Res.* **82,** 4039-4054 (1977).
9. Rossbacher, L. A. & Judson, S. *Icarus* **45,** 39-59 (1981).
10. Luchitta, B. K. *Icarus* **45,** 246-303 (1981).
11. Kuzmin, R. O. *The Cryolothosphere of Mars* (Nauka, Moscow, 1983).
12. Squyres, S. W. & Carr, M. H. *Science* **231,** 249 (1986).
13. Farmer, C. B. & Doms, P. E. *J. geophys. Res.* **84,** 2881-2888 (1979).
14. Zent, A. P., Fanale, F. P., Salvail, J. R. & Postawko, S. P. *Icarus* **67,** 19-36 (1986).
15. Ramohalli, K., Dowler, W., French, J. & Ash, R. *J. Spacecraft* **24,** 236-244 (1987).
16. Palluconi, F. D. & Kieffer, H. H. *Icarus* **45,** 415-426 (1981).
17. Jakosky, B. M. & Christensen, P. R. *J. geophys. Res.* **91,** 3547-3559 (1986).
18. Christensen, P. R. *J. geophys. Res.* **91,** 3533-3545 (1986).
19. Lachenbruch, A. H. *Bull. US geol. Surv.* 1083-A, 1-35 (1959).
20. Gold, L. W. & Lachenbruch, A. H. in *2nd Int. Conf. Permafrost* (National Academy of Sciences, 1973).
21. Ditteon, R. *J. geophys. Res.* **87,** 10197-10214 (1982).
22. Haberle, R. M. & Jakosky, B. M. *Icarus* **90,** 187-204 (1991).
23. Toon, O. B., Pollack, J. B., Ward, W., Burns, J. A. & Bilski, K. *Icarus* **44,** 552-607 (1980).
24. Carr, M. H. *Icarus* **50,** 129-139 (1982).
25. Clifford, S. M. & Hillel, D. *J. geophys. Res.* **88,** 2456-2474 (1983).
26. Jakosky, B. M. & Carr, M. H. *Nature* **315,** 559-561 (1985).
27. Fanale, F. P., Salvail, J. R., Zent, A. P. & Postawko, S. E. *Icarus* **67,** 1-18 (1986).
28. Schultz, P. H. & Lutz, A. B. *Icarus* **73,** 91-141 (1988).
29. Carr, M. H. *J. geophys. Res.* **84,** 2995-3007 (1979).
30. Kieffer, H. H. *et al. J. geophys. Res.* **82,** 4249-4291 (1977).
31. Clifford, S. M. & Bartels, C. J. *Lunar planet. Sci. XVII,* 142-143 (Lunar and Planetary Science Institute, Houston, 1986).
32. Schubert, G., Solomon, S. C., Turcotte, D. L., Drake, M. & Sleep, N. in *Mars* (eds Kieffer, H., Jakosky, B., Snyder, C. & Matthews, M.) (University of Arizona Press, Tucson, 1991).

ACKNOWLEDGEMENTS. I thank R. W. Zurek for discussion, H. H. Kieffer and S. W. Clifford for access to portions of their thermal model codes, and K. D. Keegan for model fits to the IRTM observations. Work was supported by the NASA Planetary Geology and Geophysics Program and by the California Space Institute.

Forced vortex interaction and annihilation in an active medium

J. Schütze, O. Steinbock & S. C. Müller

Max-Planck-Institut für Ernährungsphysiologie, Rheinlanddamm 201, D-4600 Dortmund 1, Germany

THE formation of spatiotemporal patterns by coupling between diffusion processes and local, nonlinear reaction kinetics has been observed in diverse systems. In one of the most familiar, the autocatalytic oxidative bromination of malonic acid (the Belousov–Zhabotinsky (BZ) reaction[1]), dynamical structures such as expanding target patterns and rotating spirals are observed. Most previous work on this system has been concerned with the autonomous dynamics of the travelling chemical waves, but more recently there has been increasing interest in the possibility of influencing the behaviour externally[2,3]. Several studies have considered the effect of electric fields on spatial patterns in the BZ system[4-8]. We have investigated previously[6] the influence of a homogeneous electric field on spiral waves. The spiral cores are of particular interest because they represent 'silent' centres in regions of pronounced dynamical activity[9]. Here we show that interactions between spiral cores can be induced and controlled by moving spirals towards each other using an applied field. Under carefully controlled conditions we have been able to induce mutual annihilation and transient coupling of spiral cores. Calculations using a simple model are able to reproduce the qualitative features of the experimental results.

The effect of electrical fields on spatial patterns in the BZ reaction was first studied by Feeney *et al.*[4] and Ortoleva[5]. Ševčiková *et al.*[7,8] found that in a small glass capillary, which